

---

# NETS: A NON-EQUILIBRIUM TRANSPORT SAMPLER

**Michael S. Albergo**

Society of Fellows  
Harvard University  
Cambridge, MA 02138, USA  
malbergo@fas.harvard.edu

**Eric Vanden-Eijnden**

Courant Institute of Mathematical Sciences  
New York University  
New York, NY 10012, USA  
eve2@cims.nyu.edu

## ABSTRACT

We propose an algorithm, termed the Non-Equilibrium Transport Sampler (NETS), to sample from unnormalized probability distributions. NETS can be viewed as a variant of annealed importance sampling (AIS) based on Jarzynski’s equality, in which the stochastic differential equation used to perform the non-equilibrium sampling is augmented with an additional learned drift term that lowers the impact of the unbiasing weights used in AIS. We show that this drift is the minimizer of a variety of objective functions, which can all be estimated in an unbiased fashion without backpropagating through solutions of the stochastic differential equations governing the sampling. We also prove that some these objectives control the Kullback-Leibler divergence of the estimated distribution from its target. NETS is shown to be unbiased and, in addition, has a tunable diffusion coefficient which can be adjusted post-training to maximize the effective sample size. We demonstrate the efficacy of the method on standard benchmarks, high-dimensional Gaussian mixture distributions, and a model from statistical lattice field theory, for which it surpasses the performances of related work and existing baselines.

## 1 INTRODUCTION

The aim of this paper is to sample probability distributions supported on  $\mathbb{R}^d$  and known only up to a normalization constant. This problem arises in a wide variety in applications, ranging from statistical physics (Faulkner & Livingstone, 2023; Wilson, 1974; Hénin et al., 2022) to Bayesian inference (Neal, 1993), and it is known to be challenging when the target distribution is not log-concave. In this situation, vanilla methods based on ergodic sampling using Markov Chain Monte Carlo (MCMC) or stochastic differential equations (SDE) such as the Langevin dynamics typically have very slow convergence rates, making them inefficient in practice.

To overcome these difficulties, a variety of more sophisticated methods have been introduced, based e.g. on importance sampling. Here we will be interested in a class of methods of this type which involve non-equilibrium sampling, by which we mean algorithms that attempt to sample from a non-stationary probability distribution. The idea is to first generate samples from a simple base distribution (e.g. a normal distribution) then push them in finite time unto samples from the target. Traditionally, this aim has been achieved by combining some transport using e.g. the Langevin dynamics with reweighing, so as to remove the bias introduced by the non-equilibrium quench. Neal’s Annealed Importance Sampling (AIS) (Neal, 2001), Sequential Monte Carlo (SMC) methods (Del Moral, 1997; Doucet et al., 2001), or continuous-time variants thereof based on Jarzynski’s equality are ways to implement this idea in practice. While these methods work better than ergodic sampling in many instances, they too can fail when the variance of the un-biasing weights become too large compared to their mean: this arises when the samples end up being too far from the target distribution at the end of the non-equilibrium quench.

This problem suggests to modify the dynamics of the samples to help them evolves towards the target during the quench. Here we propose a way to achieve this by learning an *additional drift* to include in the Langevin SDE. As we will show below, there exists a drift that removes the need for the un-biasing weights altogether, and it is the minimizer of a variety of objective functions that are amenable to empirical estimation. In practice, this offers the possibility to estimate this drift using deep learning methods. We exploit this idea here, showing that it results in an unbiased sampling

strategy in which importance weights can still be used to correct the samples exactly, but the variance of these weights can be made much smaller due to the additional transport.

To this end, our work makes the following **main contributions**:

- We present a sampling algorithm which combines annealed Langevin dynamics with learnable additional transport. The algorithm, which we call the Non-Equilibrium Transport Sampler (NETS), is shown to be unbiased through a generalization of the Jarzynski equality.
- We show that the drift coefficient contributing this additional transport is the minimizer of two separate objective functions, which can be learned without backpropagating through solutions of the SDE used for sampling.
- We show that one of these objectives, a physics informed neural network (PINN) loss, is also an *off-policy* objective, meaning that it does not need samples from the target density. In addition, this objective controls the KL-divergence between the model and its target.
- The resultant samplers can be adapted *after training* by tuning the integration time-step as well as the diffusivity to improve the sample quality, which we demonstrate on high-dimensional numerical experiments below.

## 1.1 RELATED WORK

**Dynamical Measure Transport.** Most contemporary generative models for continuous data are built upon dynamical measure transport, in which samples from a base density are mapped to samples from a target density by means of solving ordinary or stochastic differential equations (ODE/SDE) whose drift coefficients are estimable. Initial attempts to do this started with (Chen et al., 2018; Grathwohl et al., 2019). Recent work built upon these ideas by recasting the challenge of estimating the drift coefficients in these dynamical equations as a problem of quadratic regression, most notably with score-based diffusion models (Ho et al., 2020; Song et al., 2020), and since then with more general frameworks (Albergo & Vanden-Eijnden, 2022; Lipman et al., 2022; Albergo et al., 2023; Liu et al., 2022; De Bortoli et al., 2021; Neklyudov et al., 2023). Importantly, these methods work because samples from the base and the target are readily available. Here, we show that analogous equations governing those systems can lead to objective functions that can be minimized with no initial data but still allow us to exploit the expressivity of models built on dynamical transport.

**Augmenting sampling with learning.** Augmenting MCMC and importance sampling procedures with transport has been an active area of research for the past decade. Early work makes use of the independence Metropolis algorithm (Hastings, 1970; Liu, 1996), in which proposals come from a transport map (Parno & Marzouk, 2018; Noé et al., 2019; Albergo et al., 2019; Gabrié et al., 2022) that are accepted or rejected based off their likelihood ratio with the target. These methods were further improved by combining them with AIS and SMC perspectives, learning incremental maps that connect a sequence of interpolating densities between the base and target (Arbel et al., 2021; Matthews et al., 2022; Midgley et al., 2023). Similar works in the high-energy physics community posit that interleaving stochastic updates within a sequence of maps can be seen as a form of non-equilibrium sampling (Caselle et al., 2022; Bonanno et al., 2024).

Following the success of generative models built out of dynamical transport, there has been a surge of interest in applying these perspectives to sampling: Vargas et al. (2023); Berner et al. (2024)

Method	Dynamical Transport	No backprop thru time	Off-Policy Learning	Grid-Free Learning	Unbiased
FAB	×	✓	×	×	✓
DDS	✓	×	×	×	<i>Partial</i>
PIS	✓	×	×	✓	✓
CMCD	✓	<i>Partial</i>	×	×	✓
p/IDEM	✓	✓	<i>Partial</i>	✓	×
NETS-AM (ours)	✓	✓	×	✓	✓
NETS-PINN (ours)	✓	✓	✓	✓	✓

translate ideas from diffusion models to minimize the KL divergence between the model and the target, and Zhang & Chen (2021) reformulate sampling as a stochastic optimal control (SOC) problem. These approaches require backpropagating through the solution of an SDE, which is too costly in high dimensions. In addition, the methods based on SOC must start with samples from a point mass, which may be far from the target. Akhound-Sadegh et al. (2024) avoid the need to backpropagate through an SDE, but in the process introduce a bias into their objective function.

Vargas et al. (2024) establish an unbiased sampler with added transport called Controlled Monte Carlo Diffusions (CMCD) that is similar to ours. The main difference is how we learn the drift. In Vargas et al. (2024) an objective for this drift in gradient form is derived through the use of path integrals and Crook’s identity. This objective either needs backpropagating through the SDE or has to be computed with a reference measure which may make it high variance, and is done on a fixed grid. Here, through simple manipulations of Fokker-Planck equations, we propose a variety of new objective functions for the additional drift, none of which require backpropagating through the simulation. In addition, our learning can be done in a optimize-then-discretize fashion so that the sampling can be done with arbitrary step size and time-dependent diffusion after learning the model. This gives us an adaptive knob to increase performance, which we demonstrate below.

## 2 METHODS

### 2.1 SETUP AND NOTATIONS

We assume that the target distribution is absolutely continuous with respect to the Lebesgue measure on  $\mathbb{R}^d$ , with probability density function (PDF)  $\rho_1(x) = Z_1^{-1}e^{-U_1(x)}$ : here  $x \in \mathbb{R}^d$ ,  $U : \mathbb{R}^d \rightarrow \mathbb{R}$  is a known energy potential, assumed twice differentiable and bounded below, and  $Z_1 = \int_{\mathbb{R}^d} e^{-U_1(x)} dx < \infty$  is an unknown normalization constant, referred to as the partition function in physics and the evidence in statistics. Our aim is to generate samples from  $\rho_1(x)$  so as to be able to estimate expectations with respect to this density. Additionally we wish to estimate  $Z_1$ .

To this end we will use a series of time-dependent potentials  $U_t(x)$  which connects some simple  $U_0(x)$  at  $t = 0$  (e.g.  $U_0(x) = \frac{1}{2}|x|^2$ ) to  $U_1(x)$  at  $t = 1$ . For example we could use linear interpolation:

$$U_t(x) = (1 - t)U_0(x) + tU_1(x), \quad (1)$$

but other choices are possible as long as  $U_{t=0} = U_0$ ,  $U_{t=1} = U_1$ , and  $U_t(x)$  is twice differentiable in  $(t, x) \in [0, 1] \times \mathbb{R}^d$ . We assume that the time-dependent PDF associated with this potential  $U_t(x)$  is normalizable for all  $t \in [0, 1]$  and denote it as

$$\rho_t(x) = Z_t^{-1}e^{-U_t(x)}, \quad Z_t = \int_{\mathbb{R}^d} e^{-U_t(x)} dx < \infty, \quad (2)$$

so that  $\rho_{t=0}(x) = \rho_0(x)$  and  $\rho_{t=1}(x) = \rho_1(x)$ ; we also assume that  $\rho_0(x)$  is simple to sample (either directly or via MCMC or Langevin dynamics) and that its partition function  $Z_0$  is known. To simplify the notations we also introduce the free energy

$$F_t = -\log Z_t. \quad (3)$$

Note that since  $\partial_t \log F_t = -\partial_t \log \int_{\mathbb{R}^d} e^{-U_t(x)} dx = \int_{\mathbb{R}^d} \partial_t U_t(x) e^{-U_t(x)} dx / \int_{\mathbb{R}^d} e^{-U_t(x)} dx$  we have the useful identity

$$\partial_t F_t = \int_{\mathbb{R}^d} \partial_t U_t(x) \rho_t(x) dx. \quad (4)$$

### 2.2 NONEQUILIBRIUM SAMPLING WITH IMPORTANCE WEIGHTS

Annealed importance sampling uses a finite sequence of MCMC moves that satisfy detailed-balance locally in time but not globally, thereby introducing a bias that can be corrected with weights. Here we present a time-continuous variant of AIS based on Jarzynski equality that will be more useful for our purpose.

By definition of the PDF in 2,  $\nabla \rho_t(x) = -\nabla U_t(x) \rho_t(x)$  and hence, for any  $\varepsilon_t \geq 0$ , we have

$$0 = \varepsilon_t \nabla \cdot (\nabla U_t \rho_t + \nabla \rho_t). \quad (5)$$

Since we also have

$$\partial_t \rho_t = -(\partial_t U_t - \partial_t F_t) \rho_t, \quad (6)$$

we can combine these last two equations to deduce that

$$\partial_t \rho_t = \varepsilon_t \nabla \cdot (\nabla U_t \rho_t + \nabla \rho_t) - (\partial_t U_t - \partial_t F_t) \rho_t. \quad (7)$$

The effect of the last term at the right hand-side of this equation can be accounted for by using weights. To see how, notice that if we extend the phase space to  $(x, a) \in \mathbb{R}^{d+1}$  and introduce the PDF  $f_t(x, a)$  solution to the Fokker-Planck equation (FPE)

$$\partial_t f_t = \varepsilon_t \nabla \cdot (\nabla U_t f_t + \nabla f_t) + \partial_t U_t \partial_a f_t, \quad f_{t=0}(x, a) = \delta(a) \rho_0(x). \quad (8)$$

then a direct calculation using 4 (for details see Appendix 5.1) shows that

$$\rho_t(x) = \frac{\int_{\mathbb{R}} e^a f_t(x, a) da}{\int_{\mathbb{R}^{d+1}} f_t(y, a) da dy} \quad (9)$$

since the right hand-side of this equation satisfies 5 and the solutions to both 5 and 8 are unique. Therefore we can use the solution to SDE associated with the extended FPE 8 to estimate expectations with respect to  $\rho_t(x)$ :

**Proposition 1** (Jarzynski equality). *Let  $(X_t, A_t)$  solve the coupled system of SDE/ODE*

$$dX_t = -\varepsilon_t \nabla U(X_t) dt + \sqrt{2\varepsilon_t} dW_t, \quad X_0 \sim \rho_0, \quad (10)$$

$$dA_t = -\partial_t U(X_t) dt, \quad A_0 = 0, \quad (11)$$

where  $\varepsilon_t \geq 0$  is a time-dependent diffusion coefficient and  $W_t \in \mathbb{R}^d$  is the Wiener process. Then for all  $t \in [0, 1]$  and any test function  $h : \mathbb{R}^d \rightarrow \mathbb{R}$ , we have

$$\int_{\mathbb{R}^d} h(x) \rho_t(x) dx = \frac{\mathbb{E}[e^{A_t} h(X_t)]}{\mathbb{E}[e^{A_t}]}, \quad (12)$$

where the expectations at the right-hand side are taken over the law of  $(X_t, A_t)$ .

The proof of this proposition is given in Appendix 5.1 and it relies on the identity  $\int_{\mathbb{R}^d} h(x) \rho_t(x) = \int_{\mathbb{R}^{d+1}} e^a h(x) f_t(x, a) da dx / \int_{\mathbb{R}^{d+1}} f_t(x, a) da dx$  which follows from 9. The proof shows that  $\mathbb{E}[e^{A_t}] = Z_t/Z_0$ , or equivalently  $F_t = F_0 - \log \mathbb{E}[e^{A_t}]$ : this last equation for the free energy  $F_t$  is what is referred to as Jarzynski's equality.

**Remark 1.** *We stress that it is key to use the weights  $e^{A_t}$  in 12 because  $\rho_t(x)$  is not the PDF of  $X_t$  in general. Indeed, the PDF of  $X_t$  satisfies a FPE similar to 9, but without the term  $-(\partial_t U_t - \partial_t F_t) \rho_t$  at the right hand-side, and in the absence of this term the solution of the FPE is not  $\rho_t(x)$  – intuitively, the PDF of  $X_t$  lags behind  $\rho_t(x)$  when the potential  $U_t(x)$  evolves and this lag is what the weights correct for.*

It is important to realize that, while the relation 12 can be used to compute unbiased estimators of expectations, this estimator on its own can be high variance if the lag between the PDF of  $X_t$  and  $\rho_t(x)$  is too pronounced. This issue can be alleviated by using resampling methods as is done in sequential Monte Carlo (Doucet et al., 2001). Here we will solve it by adding some additional drift in 10 that will compensate for the lag the PDF of  $X_t$  and  $\rho_t(x)$ , and reduce the effect of the weights.

### 2.3 NONEQUILIBRIUM SAMPLING WITH PERFECT ADDITIONAL TRANSPORT

To see how we can add a transport term to eliminate the need of the weights, notice that, if we introduce a velocity field  $b_t(x) \in \mathbb{R}^d$  which at all times  $t \in [0, 1]$  satisfies<sup>1</sup>

$$\nabla \cdot (b_t \rho_t) = -\partial_t \rho_t, \quad (13)$$

then we can combine this equation with 5 and 6 to arrive at

$$\partial_t \rho_t = \varepsilon_t \nabla \cdot (\nabla U_t \rho_t + \nabla \rho_t) - \nabla \cdot (b_t \rho_t), \quad (14)$$

which is a standard FPE. Therefore the solution to the SDE associated with 14 allows us to sample  $\rho_t(x)$  directly (without weights). We phrase this result as:

**Proposition 2** (Sampling with perfect additional transport.). *Let  $b_t(x)$  be a solution to 13 and let  $X_t^b$  satisfy the SDE*

$$dX_t^b = -\varepsilon_t \nabla U(X_t^b) dt + b_t(X_t^b) dt + \sqrt{2\varepsilon_t} dW_t, \quad X_0^b \sim \rho_0, \quad (15)$$

<sup>1</sup>We stress that this is an equation for  $b_t(x)$  in which  $\rho_t(x)$  is fixed and given by 2.

where  $\varepsilon_t \geq 0$  is a time-dependent diffusion coefficient and  $W_t \in \mathbb{R}^d$  is the Wiener process. Then  $\rho_t(x)$  is the PDF of  $X_t^b$ , i.e. for all  $t \in [0, 1]$  and, given any test function  $h : \mathbb{R}^d \rightarrow \mathbb{R}$ , we have

$$\int_{\mathbb{R}^d} h(x) \rho_t(x) dx = \mathbb{E}[h(X_t^b)], \quad (16)$$

where the expectation on the right-hand side is taken over the law of  $(X_t^b)$ .

This proposition is proven in Appendix 5.1 and it shows that we can in principle get rid of the weights altogether by adding the drift  $b_t(x)$  in the Langevin SDE. Of course, in practice we need to estimate this drift, and also correct for sampling errors if this drift is imperfectly learned. Let us discuss this second question first, and defer the derivation of objectives to learn  $b_t(x)$  to Secs. 2.5 and 2.6.

## 2.4 NON-EQUILIBRIUM TRANSPORT SAMPLER

Let us now show that we can combine the approaches discussed in Secs. 2.2 and 2.3 to design samplers in which we use an added transport, possibly imperfect, and importance weights.

To this end, suppose that we wish to add an additional transport term  $-\nabla \cdot (\hat{b}_t \rho_t)$  in 5, where  $\hat{b}_t(x) \in \mathbb{R}^d$  is some given velocity that does not necessarily solve 13. Using the expression in 2 for  $\rho_t(x)$ , we have the identity

$$-\nabla \cdot (\hat{b}_t \rho_t) = -\nabla \cdot \hat{b}_t \rho_t + \nabla U_t \cdot \hat{b}_t \rho_t \quad (17)$$

Therefore we can rewrite 5 equivalently as

$$\partial_t \rho_t = \varepsilon_t \nabla \cdot (\nabla U_t \rho_t + \nabla \rho_t) - \nabla \cdot (\hat{b}_t \rho_t) + (\nabla \cdot \hat{b}_t - \nabla U_t - \partial_t U_t + \partial_t F_t) \rho_t. \quad (18)$$

We can now proceed as we did with 5 and extend state space to account for the effect of the terms  $(\nabla \cdot \hat{b}_t - \nabla U_t - \partial_t U_t + \partial_t F_t) \rho_t$  in this equation via weights, while having the term  $-\nabla \cdot (\hat{b}_t(x) \rho_t(x))$  contribute to some additional transport. This leads us to:

**Proposition 3** (Nonequilibrium Transport Sampler (NETS)). *Let  $(X_t^{\hat{b}}, A_t^{\hat{b}})$  solve the coupled system of SDE/ODE*

$$dX_t^{\hat{b}} = -\varepsilon_t \nabla U(X_t^{\hat{b}}) dt + \hat{b}_t(X_t^{\hat{b}}) dt + \sqrt{2\varepsilon_t} dW_t, \quad X_0^{\hat{b}} \sim \rho_0, \quad (19)$$

$$dA_t^{\hat{b}} = \nabla \cdot \hat{b}_t(X_t^{\hat{b}}) dt - \nabla U_t(X_t^{\hat{b}}) \cdot \hat{b}_t(X_t^{\hat{b}}) dt - \partial_t U_t(X_t^{\hat{b}}) dt, \quad A_0^{\hat{b}} = 0, \quad (20)$$

where  $\varepsilon_t \geq 0$  is a time-dependent diffusion coefficient and  $W_t \in \mathbb{R}^d$  is the Wiener process. Then for all  $t \in [0, 1]$  and any test function  $h : \mathbb{R}^d \rightarrow \mathbb{R}$ , we have

$$\int_{\mathbb{R}^d} h(x) \rho_t(x) dx = \frac{\mathbb{E}[e^{A_t^{\hat{b}}} h(X_t^{\hat{b}})]}{\mathbb{E}[e^{A_t^{\hat{b}}}]}, \quad (21)$$

where expectation at the right-hand side is taken over the law of  $(X_t^{\hat{b}}, A_t^{\hat{b}})$ .

This proposition is proven in Appendix 5.1. Notice that, if  $\hat{b}_t(x) = 0$ , the equations in Proposition 3 simply reduce to those in Proposition 1, whereas if  $\hat{b}_t(x) = b_t(x)$  solves 13 we can show that

$$A_t^{\hat{b}} = F_t - F_0, \quad (22)$$

i.e. the weights have zero variance and give the free energy difference. Indeed, by expanding both sides of 13 and dividing them by  $\rho_t(x) > 0$ , this equation can equivalently be written as

$$\nabla \cdot b_t - \nabla U_t \cdot b_t = \partial_t U_t - \partial_t F_t. \quad (23)$$

As a result, when  $\hat{b}_t(x) = b_t(x)$ , 20 reduces to

$$dA_t^{\hat{b}} = \partial_t F_t dt, \quad A_0^{\hat{b}} = 0, \quad (24)$$

and the solution to this equation is 22. In practice, achieving zero variance of the weights by estimating  $b_t(x)$  exactly is not generally possible, but having a good approximation of  $b_t(x)$  can help reducing this variance dramatically, as we will illustrate below via experiments.

## 2.5 ESTIMATING THE DRIFT $b_t(x)$ VIA A PINN OBJECTIVE

Equation 23 can be used to derive an objective for both  $b_t(x)$  and  $F_t$ . The reason is that in this equation the unknown  $\partial_t F_t$  can be viewed as factor that guarantees solvability: indeed, integrating both sides of 13 gives  $0 = -\partial_t \int_{\mathbb{R}^d} U_t(x) \rho_t(x) dx + \partial_t F_t$ , which, by 4, is satisfied if and only if  $F_t$  is (up to a constant fixed by  $F_0 = -\log Z_0$ ) the exact free energy 3. This offers the possibility to learn both  $b_t(x)$  and  $F_t$  variationally using an objective fitting the framework of physics informed neural networks (PINNs):

**Proposition 4** (PINN objective). *Given any  $T \in (0, 1]$  and any PDF  $\hat{\rho}_t(x) > 0$  consider the objective for  $(\hat{b}, \hat{F})$  given by:*

$$L_{PINN}^T[\hat{b}, \hat{F}] = \int_0^T \int_{\mathbb{R}^d} |\nabla \cdot \hat{b}_t(x) - \nabla U_t(x) \cdot \hat{b}_t(x) - \partial_t U_t(x) + \partial_t \hat{F}_t|^2 \hat{\rho}_t(x) dx dt. \quad (25)$$

Then  $\min_{\hat{b}, \hat{F}} L_{PINN}^T[b, F] = 0$ , and all minimizers are such that  $F_t$  is the free energy 3 and  $b_t(x)$  solves 23 for all  $t \in [0, T]$ .

This result is proven in Appendix 5.1: in practice, we will use  $T \in (0, 1]$  for annealing but ultimately we are interested in the result when  $T = 1$ . Note that since the expectation over an arbitrary  $\hat{\rho}_t(x)$  in 25, it is an off-policy objective. It is however natural to use  $\hat{\rho}_t(x) = \rho_t(x)$  since it allows us to put statistical weight in the objective precisely in the regions where we need  $b_t(x)$  to transport probability mass: we will show below how the expectation over  $\rho_t(x)$  can be estimated without bias to arrive at an empirical estimator for 25 when  $\hat{\rho}_t(x) = \rho_t(x)$ . Note also that, while minimization of the objective 25 gives an estimate  $\hat{F}_t$  of the free energy, it is not needed at sampling time when solving 19.

One advantage of the PINN objective 25 is that we know that its minimum is zero, and hence we can track its value to monitor convergence when minimizing 25 by gradient descent as we do below. Another advantage of the loss 25 is that it controls the quality of the transport as measured by the Kullback-Leibler divergence:

**Proposition 5** (KL control). *Let  $\hat{\rho}_t$  be the solution to the transport equation*

$$\partial_t \hat{\rho}_t = -\nabla \cdot (\hat{b}_t \hat{\rho}_t), \quad \hat{\rho}_{t=0} = \rho_0 \quad (26)$$

where  $\hat{b}_t(x)$  is some predefined velocity field. Then, given any estimate  $\hat{F}_t$  of the exact free energy  $F_t$ , we have

$$D_{KL}(\hat{\rho}_{t=1} || \rho_1) \leq \sqrt{L_{PINN}^{T=1}(\hat{b}, \hat{F})}. \quad (27)$$

This proposition is proven in Appendix 5.1.

## 2.6 ESTIMATING THE DRIFT $b_t(x) = \nabla \phi_t(x)$ VIA ACTION MATCHING (AM)

In general 13 is solved by many  $b_t(x)$ . One way to get a unique (up to a constant in space and time) solution to this equation is to impose that the velocity be in gradient form, i.e. set  $b_t(x) = \nabla \phi_t(x)$  for some scalar-valued potential  $\phi_t(x)$ . If we do so, 13 can be written as  $\nabla \cdot (\nabla \phi_t(x) \rho_t) = -\partial_t \rho_t$ , and it is easy to see that at all times  $t \in [0, 1]$  the solution to this equation minimizes over  $\hat{\phi}_t$  the objective

$$\begin{aligned} & \int_{\mathbb{R}^d} \left[ \frac{1}{2} |\nabla \hat{\phi}_t(x)|^2 \rho_t(x) - \phi_t(x) \partial_t \rho_t(x) \right] dx \\ & = \int_{\mathbb{R}^d} \left[ \frac{1}{2} |\nabla \hat{\phi}_t(x)|^2 + \partial_t U_t(x) - \partial_t F_t \right] \rho_t(x) dx. \end{aligned} \quad (28)$$

If we use 4 to set  $\partial_t F_t = \int_{\mathbb{R}^d} \partial_t U_t(x) \rho_t(x) dx$  we can use the objective at the right hand-side of 28 to learn  $\phi_t(x)$  locally in time (or globally if we integrate this objective on  $t \in [0, 1]$ ). Alternatively, we can integrate the objective at the left hand-side of 28 over  $t \in [0, T]$  and use integration by parts for the term involving  $\partial_t \rho_t(x)$  to arrive at:

**Proposition 6** (Action Matching objective). *Given any  $T \in (0, 1]$  consider the objective for  $\hat{\phi}_t(x)$ :*

$$L_{AM}^T[\hat{\phi}] = \int_0^T \int_{\mathbb{R}^d} \left[ \frac{1}{2} |\nabla \hat{\phi}_t(x)|^2 + \partial_t \phi_t(x) \right] \rho_t(x) dx dt + \int_{\mathbb{R}^d} [\phi_0(x) \rho_0(x) - \phi_T(x) \rho_T(x)] dx. \quad (29)$$

Then the minimizer  $\phi_t(x)$  of 25 is unique (up to a constant) and  $b_t(x) = \nabla\phi_t(x)$  satisfies 13 for all  $t \in [0, T]$ .

This proposition is proven in Appendix 5.1. This objective is analogous to the loss presented in Neklyudov et al. (2023), but adapted to the sampling problem. In practice, we will use again  $T \in (0, 1]$  for annealing, but ultimately we are interested in the result at  $T = 1$ . Note that, unlike with the PINN objective 25, it is crucial that we use the correct  $\rho_t(x)$  in the AM objective 29: that is, unlike 25, 29 cannot be turned into an off-policy objective.

**Remark 2.** If we use  $\hat{b}_t(x) = \nabla\hat{\phi}_t(x)$  in the SDEs in 19 and 20, we need to estimate  $\nabla \cdot \hat{b}_t(x) = \Delta\hat{\phi}_t(x)$ . Fortunately, when  $\varepsilon_t > 0$ , the calculation of this Laplacian can be avoided by using the following alternative equation for  $A_t^{\hat{b}}$ :

$$A_t^{\hat{b}} = \frac{1}{\varepsilon_t} [\phi_t(X_t^{\hat{b}}) - \phi_0(X_0^{\hat{b}})] - B_t, \quad (30)$$

where

$$dB_t = \partial_t U_t(X_t^{\hat{b}}) dt + \frac{1}{\varepsilon_t} \partial_t \phi_t(X_t^{\hat{b}}) + \frac{1}{\varepsilon_t} |\nabla\phi_t(X_t^{\hat{b}})|^2 dt + \sqrt{\frac{2}{\varepsilon_t}} \nabla\phi_t(X_t^{\hat{b}}) \cdot dW_t. \quad (31)$$

This equation is derived in Appendix 5.1.

### 3 IMPLEMENTATION

The PINN objective 25 can be written as

$$L_{\text{PINN}}^T[\hat{b}, \hat{F}] = \int_0^T \mathbb{E} \left[ |\nabla \cdot \hat{b}_t(\hat{x}_t) - \nabla U_t(\hat{x}_t) \cdot \hat{b}_t(\hat{x}_t) - \partial_t U_t(\hat{x}_t) + \partial_t \hat{F}_t|^2 \right] dt \quad (32)$$

where the expectation is taken over  $\hat{x}_t$  drawn from  $\hat{\rho}_t(x)$ , and it can be estimated empirically over a population of such samples. This is the *off-policy* variant of the PINN objective, and it is perfectly valid, but may be inefficient for learning  $\hat{b}_t$  over the support necessary for the problem. If we decide instead to set  $\hat{\rho}_t(x) = \rho_t(x)$ , since the SDEs in 19 and 20 can be used with any  $\hat{b}_t(x)$  to estimate expectation over  $\rho_t(x)$  via 21, we can write the PINN objective on-policy as

$$L_{\text{PINN}}^T[\hat{b}, \hat{F}] = \int_0^T \frac{1}{\mathbb{E}[e^{A_t^{\hat{b}}}] } \mathbb{E} \left[ e^{A_t^{\hat{b}}} |\nabla \cdot \hat{b}_t(X_t^{\hat{b}}) - \nabla U_t(X_t^{\hat{b}}) \cdot \hat{b}_t(X_t^{\hat{b}}) - \partial_t U_t(X_t^{\hat{b}}) + \partial_t \hat{F}_t|^2 \right] dt \quad (33)$$

These expectations can be estimated empirically over a population of solutions to 19 and 20. Crucially, since we can switch from off-policy to on-policy after taking the gradient of the PINN objective, *when computing the gradient of 33 over  $\hat{b}_t(x)$ ,  $(X_t^{\hat{b}}, A_t^{\hat{b}})$  can be considered independent of  $\hat{b}_t(x)$  and do not need to be differentiated over.* In other words, the method is simulation-free even if used on-policy, i.e. even though it uses the current value of  $\hat{b}_t$  to estimate the loss and its gradient.

Learning  $b_t(x)$  and  $F_t$  for  $t \in [0, 1]$  from the start can be challenging if the initial  $\hat{b}_t(x)$  is far from exact and the weights gets large variance as  $t$  increases. This problem can be alleviated by estimating  $b_t(x)$  sequentially. In practice, this amounts to annealing  $T$  from a small initial value to  $T = 1$ , in such a way that  $b_t(x)$  is learned sufficiently accurately so that variance of the weights remains small. This variance can be estimated on the fly, which also give us an estimate of the effective sample size (ESS) of the population at all times  $t \in [0, 1]$ .

Note that we can also employ resampling strategies of the type used in SMC to keep the variance of the weights low Doucet et al. (2001); Bolić et al. (2004).

We can proceed similarly with the AM loss 29 by rewriting it as

$$L_{\text{AM}}^T[\hat{\phi}] = \int_0^T \frac{\mathbb{E} [e^{A_t^{\hat{b}}} [\frac{1}{2} |\nabla\hat{\phi}_t(X_t^{\hat{b}})|^2 + \partial_t \phi_t(X_t^{\hat{b}})]]}{\mathbb{E}[e^{A_t^{\hat{b}}}] } dt + \frac{\mathbb{E}[e^{A_0^{\hat{b}}} \phi_0(X_0^{\hat{b}})]}{\mathbb{E}[e^{A_0^{\hat{b}}}] } - \frac{\mathbb{E}[e^{A_T^{\hat{b}}} \phi_T(X_T^{\hat{b}})]}{\mathbb{E}[e^{A_T^{\hat{b}}}] }. \quad (34)$$

These expectations can be estimated empirically over solutions to 19 and 20 with  $\hat{b}_t(x) = \nabla\hat{\phi}_t(x)$ . The above implementation is detailed in Algorithm 1 in Appendix 5.2.

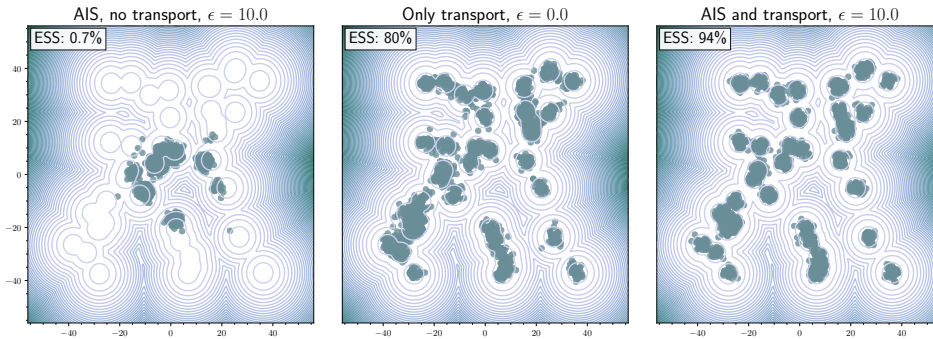


Figure 1: Comparison of the performance of annealed Langevin dynamics alone, transport alone, and annealed Langevin coupled with transport when sampling the 40-mode GMM from Midgley et al. (2023). **Left:** Annealed Langevin run for 250 steps with  $\varepsilon_t = 10.0$ , failing to capture the modes with 0% ESS. **Center:** Learning using the PINN loss and sampling with  $\varepsilon_t = 0$  achieves an ESS of 80%. **Right:** Learning using the PINN loss and sampling with  $\varepsilon_t = 10.0$  achieves an ESS of 94%.

## 4 NUMERICAL EXPERIMENTS

In what follows, we test the NETS method, for both the PINN objective 25 and the action matching objective 29, on standard challenging sampling benchmarks. We then study how the method scales in comparison to baselines, particularly AIS on its own, by testing it on an increasingly high dimensional Gaussian Mixture Models (GMM). Following that, we show that it has orders of magnitude better statistical efficiency as compared to AIS on its own when applied to the study of lattice field theories, even past the phase transition of these theories and in 400 dimensions (an  $L = 20 \times L = 20$  lattice).

### 4.1 40-MODE GAUSSIAN MIXTURE

A common benchmark for machine learning augmented samplers that originally appeared in the paper introducing Flow Annealed Importance Sampling Bootstrap (FAB) Midgley et al. (2023) is a 40-mode GMM in 2-dimensions for which the means of the mixture components span from  $-40$  to  $40$ . The high variance and many wells make this problem challenging for re-weighting or locally updating MCMC processes. We choose as a time dependent potential  $U_t(x)$  the linear interpolation 1 with  $U_0$  the potential for a standard multivariate Gaussian with standard deviation scale  $\sigma = 2$ .

Algorithm	GMM ( $d = 2$ )	
	ESS $\uparrow$	$\mathcal{W}_2 \downarrow$
FAB	$0.653 \pm 0.017$	$12.0 \pm 5.73$
PIS	$0.295 \pm 0.018$	$7.64 \pm 0.92$
DDS	$0.687 \pm 0.208$	$9.31 \pm 0.82$
pDEM	$0.634 \pm 0.084$	$12.20 \pm 0.14$
iDEM	$0.734 \pm 0.092$	$7.42 \pm 3.44$
NETS-AM (ours)	$0.808 \pm 0.031$	$3.89 \pm 0.22$
NETS-PINN (ours)	<b><math>0.941 \pm 0.002</math></b>	<b><math>3.28 \pm 0.68</math></b>
NETS-PINN-resample (ours)	<b><math>0.987 \pm 0.007</math></b>	<b><math>3.16 \pm 0.039</math></b>

Table 1: Performance of NETS in terms of ESS and 2-Wasserstein metrics for 40-mode GMM ( $d = 2$ ) with comparative results quoted from Akhound-Sadegh et al. (2024) for reproducibility.

2000 generated samples as well as the 2-Wasserstein ( $\mathcal{W}_2$ ) distance between the model and the target. As noted in Table 1, all proposed variants of NETS outperform existing methods. In addition, because our method can be turned into an SMC method by including resampling during the generation, we can push the acceptance rate of the same learned PINN model to nearly 100% by using a single resampling step when the ESS of the walkers dropped below 95%. NETS uses 250 sampling steps and an  $\varepsilon_t = 10.0$  in the SDE.

We train a simple feed-forward neural network of width 256 against both the PINN objective 25, parameterizing  $(\hat{b}, \hat{F})$ , or the action matching objective 29, parameterizing  $\hat{\phi}$ . We compare the learned model from both objectives to recent related literature: FAB, Path Integral Sampler (PIS) (Zhang & Chen, 2021), Denoising Diffusion Sampler (DDS) (Vargas et al., 2023), and Denoising Energy Matching (pDEM, iDEM) (Akhound-Sadegh et al., 2024). For reproducibility with the benchmarks provided in the latter method, we compute the effective sample size (ESS) estimated from



## 4.2 10-D FUNNEL DISTRIBUTION

We next test NETS on Neal’s funnel, a challenging synthetic target distribution which exhibits correlations at different scales across its 10 dimensions. The definitions of the target density and the interpolating potential are given in Appendix 5.2. Heuristically, the first dimension is Gaussian with variance  $\sigma^2 = 9$ , and the other 9 dimensions are conditionally Gaussian with variance  $\exp(x_0)$ , creating the funnel.

We again parameterize  $(\hat{b}, \hat{F})$  or  $\hat{\phi}$  using simple feed forward neural networks, this time of hidden size 512. We use 200 sampling steps and a mild diffusion coefficient of  $\varepsilon_t = 0.3$  to sample from the model. Following Blessing et al. (2024), we compute the maximum mean discrepancy (MMD) between 10000 samples from the model and 10000 samples from the target and compare to related methods in Table 2. NETS matches the best performing predecessors, and, when using a single resampling step during generation when the ESS drops below 70%, surpasses them.

Funnel ( $d = 10$ )	
Algorithm	MMD ↓
FAB (Midgley et al., 2023)	<b>0.032 ± 0.000</b>
GMMVI (Arenz et al., 2023)	<b>0.031 ± 0.000</b>
PIS (Zhang & Chen, 2022)	--
DDS (Vargas et al., 2023)	0.172 ± 0.031
AFT (Arbel et al., 2021)	0.159 ± 0.010
CRAFT (Arbel et al., 2021)	0.115 ± 0.003
NETS-AM (ours)	0.041 ± 0.001
NETS-PINN (ours)	<b>0.031 ± 0.002</b>
NETS-PINN-resample (ours)	<b>0.022 ± 0.002</b>

Table 2: Performance of NETS on the Neal’s Funnel distribution, measured in maximum mean discrepancy from the true distribution for reproducibility with the numbers quoted from Blessing et al. (2024).

## 4.3 SCALING ON HIGH-DIMENSIONAL GMMs

In order to demonstrate that the method generalizes to high dimension, we study sampling from multimodal GMMs in higher and higher dimensions and observe how the performance scales. In addition we are curious to understand how the factor in the sampling SDE coming from annealed Langevin dynamics,  $\nabla U$ , interacts with the learned drift  $\hat{b}$  or  $\nabla \hat{\phi}$  as we change the diffusivity. We construct 8-mode target GMMs in  $d = 36, 64, 128, 200$  dimensions and learn  $\hat{b}$  with the PINN loss in each scenario. We use the same feed forward neural network of width 512 and depth 4 to parameterize

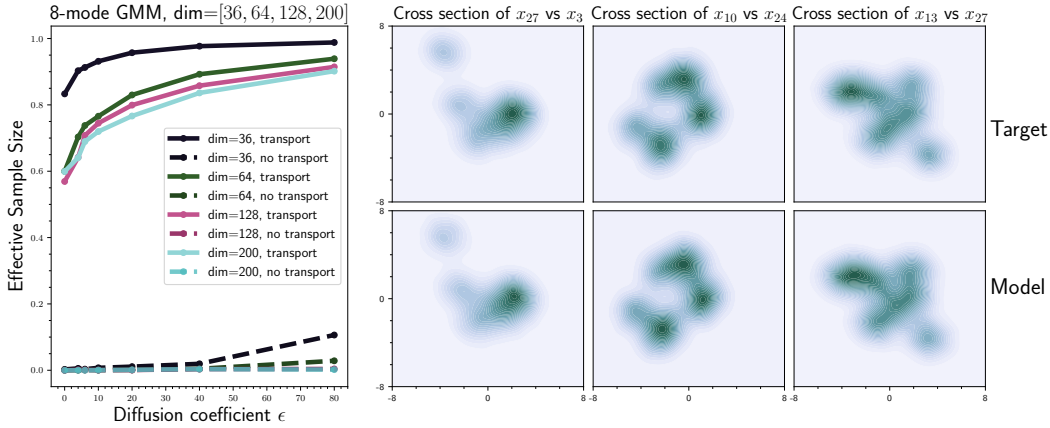


Figure 2: Demonstration of high-dimensional sampling with our method using the PINN loss in 25 and a study of how diffusivity impacts performance, with and without transport. **Left:** NETS can achieve high ESS through transport alone, and the effect of increased diffusivity has more of a positive effect on performance with sampling than without. AIS cannot achieve ESS above  $\approx 0$  in high dimension. **Right:** Kernel density estimates of  $2-d$  cross sections of the high-dimensional, multimodal distribution arising from the model and ground truth.

both  $\hat{b}$  and  $\hat{F}$  for all dimensions tested and train for 4000 training iterations. Figure 2 summarizes the results. On the left plot, we note that AIS on its own cannot produce any effective samples, while even in 200 dimensions, NETS works with transport alone with 60% ESS. As we increase the diffusivity  $\varepsilon_t$  and therefore the effect of the Langevin term coming from the gradient of the potential, we note all the methods converge to nearly independent sampling, and the discrepancy in performance

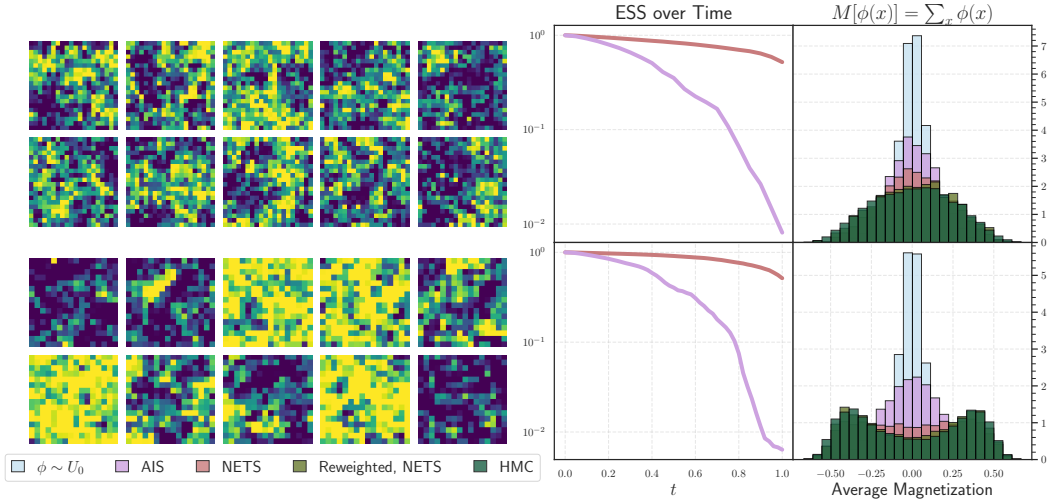


Figure 3: Comparison of the performance of NETS to AIS on two different settings for the study of  $\varphi^4$  theory. **Top row, left:** 10 example generative lattice configurations with parameters  $L = 20$ ,  $m^2 = -1.0$ ,  $\lambda = 0.9$ , which demarcates the phase transition to the antiferromagnetic phase. **Top row, right:** Performance of AIS (purple curve) vs. NETS (red curve) in terms of effective sample size over time of integration  $t$ , and a histogram of the average magnetization of 4000 lattice configurations, sampled with AIS, NETS, and HMC (superposed in this order). Note that NETS is closer to the HMC target and re-weights correctly. Re-weighted AIS was not plotted because the weights were too high variance. **Bottom row:** Equivalent setup for  $L = 16$ ,  $m^2 = -1.0$ ,  $\lambda = 0.8$ , past the phase transition and into the ordered phase. Note that the field configurations generated by NETS are either all positive across lattice sites or all negative. AIS fails to sample the correct distribution, and its weights are too high variance to be used on the histogram.

across dimensions is diminished. Note that the caveat to achieve this is that the step size in the SDE integrator must be taken smaller to accommodate the increased diffusivity, especially for the  $\varepsilon_t = 80$  data point. The number of sampling steps used to discretize the SDEs in these experiments ranged from  $K = 200$  for  $\varepsilon_t = 0$  up to  $K = 2000$  for  $\varepsilon_t = 80$ . Nonetheless, it suggests that diffusion can be more helpful when there is already some successful transport than without.

#### 4.4 LATTICE $\varphi^4$ THEORY

We next apply NETS to the simulation of a statistical lattice field theory at and past the phase transition from which the lattice goes from disordered, to semi-ordered, to fully ordered (neighboring sites are highly correlated to be of the same sign and magnitude). We study the lattice  $\varphi^4$  theory in  $D = 2$  spacetime dimensions. The random variables in this circumstance are field configurations  $\varphi \in \mathbb{R}^{L \times L}$ , where  $L$  is the extent of space and time. The interpolating energy function under which we seek to sample is defined as:

$$U_t(\varphi) = \sum_x \left[ -2 \sum_{\mu} \varphi_x \varphi_{x+\mu} \right] + (2D + m_t^2) \varphi_x^2 + \lambda_t \varphi_x^4, \quad (35)$$

where summation over  $x$  indicates summation over the lattices sites, and  $m_t^2$  and  $\lambda_t$  are time dependent parameters of the theory that define the phase of the lattice (ranging from disordered to ordered, otherwise known as magnetized). A derivation of this energy function is given in Appendix 5.5.1. Importantly, sampling the lattice configurations becomes challenging when approaching the phase transition between the disordered and ordered phases. As an example, we identify the phase transition on  $L = 16$  ( $d = 256$ ) and  $L = 20$  ( $d = 400$ ) lattices and run NETS with the action matching loss, with  $\hat{\phi}_t$  a simple feed forward neural network. We use the free theory  $\lambda_0 = 0$  as the base distribution under which we initially draw samples. The definition of the target parameter values  $m_1^2, \lambda_1$  both at the phase transition and in the ordered phase are given in the Appendix 5.5.1. In Figure 3, the top row shows samples from NETS for  $L = 20$  at the phase transition, where correlations begin to appear in

---

the lattice configurations. NETS is almost 2 orders of magnitude more statistically efficient than AIS in sampling at the critical point, as seen in the plot showing ESS over time. Note also that NETS can produce unbiased estimates of the magnetization as compared to a Hybrid Monte Carlo (HMC) ground truth. The bottom row shows samples past the phase transition and into the ordered phase, where the lattices begin to take on either all positive or all negative values. Again in this regime, NETS is nearly 2 orders of magnitude more statistically efficient.

While NETS performs significantly better than conventional annealed samplers on the challenging field theory problem, algorithms built out of dynamical transport still experience slowdowns near phase transitions because of the difficulty of resolving the dynamics of the integrators near these critical points. As such, we need to use 1500-2000 steps in the integrator to properly resolve the dynamics of the SDE.

## ACKNOWLEDGEMENTS

We thank Francisco Vargas and Lee Cheuk-Kit for helpful discussions on related work. MSA is supported by a Junior Fellowship from the Harvard Society of Fellows and the ONR project under the Vannevar Bush award “Mathematical Foundations and Scientific Applications of Machine Learning”. EVE is supported by the National Science Foundation under Awards DMR1420073, DMS-2012510, and DMS-2134216, by the Simons Collaboration on Wave Turbulence, Grant No. 617006, and by a Vannevar Bush Faculty Fellowship.

## REFERENCES

- Tara Akhound-Sadegh, Jarrid Rector-Brooks, Joey Bose, Sarthak Mittal, Pablo Lemos, Cheng-Hao Liu, Marcin Sendera, Siamak Ravanbakhsh, Gauthier Gidel, Yoshua Bengio, Nikolay Malkin, and Alexander Tong. Iterated denoising energy matching for sampling from boltzmann densities. In Ruslan Salakhutdinov, Zico Kolter, Katherine Heller, Adrian Weller, Nuria Oliver, Jonathan Scarlett, and Felix Berkenkamp (eds.), *Proceedings of the 41st International Conference on Machine Learning*, volume 235 of *Proceedings of Machine Learning Research*, pp. 760–786. PMLR, 21–27 Jul 2024. URL <https://proceedings.mlr.press/v235/akhound-sadegh24a.html>.
- M. S. Albergo, G. Kanwar, and P. E. Shanahan. Flow-based generative models for markov chain monte carlo in lattice field theory. *Phys. Rev. D*, 100:034515, Aug 2019. doi: 10.1103/PhysRevD.100.034515. URL <https://link.aps.org/doi/10.1103/PhysRevD.100.034515>.
- Michael S Albergo and Eric Vanden-Eijnden. Building normalizing flows with stochastic interpolants. In *The Eleventh International Conference on Learning Representations*, 2022.
- Michael S Albergo, Nicholas M Boffi, and Eric Vanden-Eijnden. Stochastic interpolants: A unifying framework for flows and diffusions. *arXiv preprint arXiv:2303.08797*, 2023.
- Michael Arbel, Alexander G. D. G. Matthews, and Arnaud Doucet. Annealed flow transport monte carlo. In *Proceedings of the 38th International Conference on Machine Learning*, Proceedings of Machine Learning Research, 18–24 Jul 2021.
- Oleg Arenz, Philipp Dahlinger, Zihan Ye, Michael Volpp, and Gerhard Neumann. A unified perspective on natural gradient variational inference with gaussian mixture models. *Transactions on Machine Learning Research*, 2023. ISSN 2835-8856. URL <https://openreview.net/forum?id=tLBjsX4tjs>.
- Julius Berner, Lorenz Richter, and Karen Ullrich. An optimal control perspective on diffusion-based generative modeling, 2024. URL <https://arxiv.org/abs/2211.01364>.
- Denis Blessing, Xiaogang Jia, Johannes Esslinger, Francisco Vargas, and Gerhard Neumann. Beyond ELBOs: A large-scale evaluation of variational methods for sampling. In Ruslan Salakhutdinov, Zico Kolter, Katherine Heller, Adrian Weller, Nuria Oliver, Jonathan Scarlett, and Felix Berkenkamp (eds.), *Proceedings of the 41st International Conference on Machine Learning*, volume 235 of *Proceedings of Machine Learning Research*, pp. 4205–4229. PMLR, 21–27 Jul 2024. URL <https://proceedings.mlr.press/v235/blessing24a.html>.

- 
- Miodrag Bolić, Petar M. Djurić, and Sangjin Hong. Resampling algorithms for particle filters: A computational complexity perspective. *EURASIP Journal on Advances in Signal Processing*, 2004 (15):403686, 2004. doi: 10.1155/S1110865704405149. URL <https://doi.org/10.1155/S1110865704405149>.
- Claudio Bonanno, Alessandro Nada, and Davide Vadicchino. Mitigating topological freezing using out-of-equilibrium simulations. *Journal of High Energy Physics*, 2024(4):126, 2024. doi: 10.1007/JHEP04(2024)126. URL [https://doi.org/10.1007/JHEP04\(2024\)126](https://doi.org/10.1007/JHEP04(2024)126).
- Michele Caselle, Elia Cellini, Alessandro Nada, and Marco Panero. Stochastic normalizing flows as non-equilibrium transformations. *Journal of High Energy Physics*, 2022(7):15, 2022. doi: 10.1007/JHEP07(2022)015. URL [https://doi.org/10.1007/JHEP07\(2022\)015](https://doi.org/10.1007/JHEP07(2022)015).
- Ricky T. Q. Chen, Yulia Rubanova, Jesse Bettencourt, and David K Duvenaud. Neural ordinary differential equations. In S. Bengio, H. Wallach, H. Larochelle, K. Grauman, N. Cesa-Bianchi, and R. Garnett (eds.), *Advances in Neural Information Processing Systems*, volume 31. Curran Associates, Inc., 2018. URL [https://proceedings.neurips.cc/paper\\_files/paper/2018/file/69386f6bb1dfed68692a24c8686939b9-Paper.pdf](https://proceedings.neurips.cc/paper_files/paper/2018/file/69386f6bb1dfed68692a24c8686939b9-Paper.pdf).
- Valentin De Bortoli, James Thornton, Jeremy Heng, and Arnaud Doucet. Diffusion schrödinger bridge with applications to score-based generative modeling. In *Advances in Neural Information Processing Systems*, volume 34, pp. 17695–17709, 2021.
- Pierre Del Moral. Nonlinear filtering: Interacting particle resolution. *Comptes Rendus de l'Académie des Sciences - Series I - Mathematics*, 325(6):653–658, 1997. ISSN 0764-4442. doi: [https://doi.org/10.1016/S0764-4442\(97\)84778-7](https://doi.org/10.1016/S0764-4442(97)84778-7). URL <https://www.sciencedirect.com/science/article/pii/S0764444297847787>.
- Arnaud Doucet, Nando de Freitas, and Neil J. Gordon (eds.). *Sequential Monte Carlo Methods in Practice*. Statistics for Engineering and Information Science. Springer, 2001. ISBN 978-1-4419-2887-0. doi: 10.1007/978-1-4757-3437-9. URL <https://doi.org/10.1007/978-1-4757-3437-9>.
- Michael F. Faulkner and Samuel Livingstone. Sampling algorithms in statistical physics: a guide for statistics and machine learning, 2023. URL <https://arxiv.org/abs/2208.04751>.
- Marylou Gabrié, Grant M. Rotskoff, and Eric Vanden-Eijnden. Adaptive monte carlo augmented with normalizing flows. *Proceedings of the National Academy of Sciences*, 119(10):e2109420119, 2022. doi: 10.1073/pnas.2109420119. URL <https://www.pnas.org/doi/abs/10.1073/pnas.2109420119>.
- Will Grathwohl, Ricky T. Q. Chen, Jesse Bettencourt, and David Duvenaud. Scalable reversible generative models with free-form continuous dynamics. In *International Conference on Learning Representations*, 2019. URL <https://openreview.net/forum?id=rJxgknCcK7>.
- W. K. Hastings. Monte carlo sampling methods using markov chains and their applications. *Biometrika*, 57(1):97–109, 1970. ISSN 00063444, 14643510. URL <http://www.jstor.org/stable/2334940>.
- Jonathan Ho, Ajay Jain, and Pieter Abbeel. Denoising diffusion probabilistic models. In *Advances in neural information processing systems*, volume 33, pp. 6840–6851, 2020.
- Jérôme Hénin, Tony Lelièvre, Michael R. Shirts, Omar Valsson, and Lucie Delemotte. Enhanced sampling methods for molecular dynamics simulations [article v1.0]. *Living Journal of Computational Molecular Science*, 4(1):1583, Dec. 2022. doi: 10.33011/livecoms.4.1.1583. URL <https://livecomsjournal.org/index.php/livecoms/article/view/v4i1e1583>.
- Yaron Lipman, Ricky TQ Chen, Heli Ben-Hamu, Maximilian Nickel, and Matthew Le. Flow matching for generative modeling. In *The Eleventh International Conference on Learning Representations*, 2022.
- Jun S. Liu. Metropolisized independent sampling with comparisons to rejection sampling and importance sampling. *Statistics and Computing*, 6(2):113–119, 1996. doi: 10.1007/BF00162521. URL <https://doi.org/10.1007/BF00162521>.

- 
- Xingchao Liu, Chengyue Gong, and Qiang Liu. Flow straight and fast: Learning to generate and transfer data with rectified flow. In *The Eleventh International Conference on Learning Representations*, 2022.
- Alexander G. D. G. Matthews, Michael Arbel, Danilo J. Rezende, and Arnaud Doucet. Continual repeated annealed flow transport monte carlo. In *Proceedings of the 39th International Conference on Machine Learning*, Proceedings of Machine Learning Research, Jul 2022.
- Laurence Illing Midgley, Vincent Stimper, Gregor N. C. Simm, Bernhard Schölkopf, and José Miguel Hernández-Lobato. Flow annealed importance sampling bootstrap. In *The Eleventh International Conference on Learning Representations*, 2023. URL <https://openreview.net/forum?id=XCTVFJwS9LJ>.
- Radford M. Neal. Probabilistic inference using markov chain monte carlo methods. Technical Report CRG-TR-93-1, Department of Computer Science, University of Toronto, September 1993.
- Radford M. Neal. Annealed importance sampling. *Statistics and Computing*, 11(2):125–139, 2001. doi: 10.1023/A:1008923215028. URL <https://doi.org/10.1023/A:1008923215028>.
- Kirill Neklyudov, Rob Brekelmans, Daniel Severo, and Alireza Makhzani. Action matching: Learning stochastic dynamics from samples. In Andreas Krause, Emma Brunskill, Kyunghyun Cho, Barbara Engelhardt, Sivan Sabato, and Jonathan Scarlett (eds.), *Proceedings of the 40th International Conference on Machine Learning*, volume 202 of *Proceedings of Machine Learning Research*, pp. 25858–25889. PMLR, 23–29 Jul 2023. URL <https://proceedings.mlr.press/v202/neklyudov23a.html>.
- Frank Noé, Simon Olsson, Jonas Köhler, and Hao Wu. Boltzmann generators: Sampling equilibrium states of many-body systems with deep learning. *Science*, 365(6457):eaaw1147, 2019. doi: 10.1126/science.aaw1147. URL <https://www.science.org/doi/abs/10.1126/science.aaw1147>.
- Matthew D. Parno and Youssef M. Marzouk. Transport map accelerated markov chain monte carlo. *SIAM/ASA Journal on Uncertainty Quantification*, 6(2):645–682, 2018. doi: 10.1137/17M1134640. URL <https://doi.org/10.1137/17M1134640>.
- Yang Song, Jascha Sohl-Dickstein, Diederik P Kingma, Abhishek Kumar, Stefano Ermon, and Ben Poole. Score-based generative modeling through stochastic differential equations. *arXiv preprint arXiv:2011.13456*, 2020.
- Francisco Vargas, Will Sussman Grathwohl, and Arnaud Doucet. Denoising diffusion samplers. In *The Eleventh International Conference on Learning Representations*, 2023. URL <https://openreview.net/forum?id=8pvnfTAbu1f>.
- Francisco Vargas, Shreyas Padhy, Denis Blessing, and Nikolas Nüsken. Transport meets variational inference: Controlled monte carlo diffusions. In *The Twelfth International Conference on Learning Representations*, 2024. URL <https://openreview.net/forum?id=PP1rudnxiW>.
- Kenneth G. Wilson. Confinement of quarks. *Phys. Rev. D*, 10:2445–2459, Oct 1974. doi: 10.1103/PhysRevD.10.2445. URL <https://link.aps.org/doi/10.1103/PhysRevD.10.2445>.
- Qinsheng Zhang and Yongxin Chen. Path integral sampler: A stochastic control approach for sampling. In *International Conference on Learning Representations*, 2021.
- Qinsheng Zhang and Yongxin Chen. Path integral sampler: A stochastic control approach for sampling. In *International Conference on Learning Representations*, 2022. URL [https://openreview.net/forum?id=\\_uCb2ynRu7Y](https://openreview.net/forum?id=_uCb2ynRu7Y).

## 5 APPENDIX

### 5.1 PROOFS OF SEC. 2

Here we provide the proofs of the statements made in Sec. 2 which, for the reader convenience, we recall.

**Proposition 1** (Jarzynski equality). *Let  $(X_t, A_t)$  solve the coupled system of SDE/ODE*

$$dX_t = -\varepsilon_t \nabla U(X_t) dt + \sqrt{2\varepsilon_t} dW_t, \quad X_0 \sim \rho_0, \quad (10)$$

$$dA_t = -\partial_t U(X_t) dt, \quad A_0 = 0, \quad (11)$$

where  $\varepsilon_t \geq 0$  is a time-dependent diffusion coefficient and  $W_t \in \mathbb{R}^d$  is the Wiener process. Then for all  $t \in [0, 1]$  and any test function  $h : \mathbb{R}^d \rightarrow \mathbb{R}$ , we have

$$\int_{\mathbb{R}^d} h(x) \rho_t(x) dx = \frac{\mathbb{E}[e^{A_t} h(X_t)]}{\mathbb{E}[e^{A_t}]}, \quad (12)$$

where the expectations at the right-hand side are taken over the law of  $(X_t, A_t)$ .

*Proof.* By definition of the PDF in 2,  $\nabla \rho_t(x) = -\nabla U_t(x) \rho_t(x)$  and hence, for any  $\varepsilon_t \geq 0$ , we have

$$0 = \varepsilon_t \nabla \cdot (\nabla U_t \rho_t + \nabla \rho_t). \quad (36)$$

We also have

$$\partial_t \rho_t = -(\partial_t U_t - \partial_t F_t) \rho_t. \quad (37)$$

Combining these last two equations to deduce that

$$\partial_t \rho_t = \varepsilon_t \nabla \cdot (\nabla U_t \rho_t + \nabla \rho_t) - (\partial_t U_t - \partial_t F_t) \rho_t. \quad (38)$$

Consider now the PDF  $f_t(x, a)$  in the extended state space  $(x, a) \in \mathbb{R}^d$  defined as the solution to the FPE

$$\partial_t f_t = \varepsilon_t \nabla \cdot (\nabla U_t f_t + \nabla f_t) + \partial_t U_t \partial_a f_t, \quad f_{t=0}(x, a) = \delta(a) \rho_0(x), \quad (39)$$

and let

$$g_t(x) = \int_{\mathbb{R}} e^a g_t(x, a) da. \quad (40)$$

We can derive an equation for  $g_t(x)$  by multiplying both sides of 39 by  $e^a$  and integrating over  $a \in \mathbb{R}$ . Using

$$\begin{aligned} \int_{\mathbb{R}} e^a \partial_t f_t(x, a) da &= \partial_t \int_{\mathbb{R}} e^a f_t(x, a) da = \partial_t g_t \\ \int_{\mathbb{R}} e^a \varepsilon_t \nabla \cdot (\nabla U_t f_t + \nabla f_t) da &= \varepsilon_t \nabla \cdot \left( \nabla U_t \int_{\mathbb{R}} e^a f_t(x, a) da + \nabla \int_{\mathbb{R}} e^a f_t(x, a) da \right) \\ &= \varepsilon_t \nabla \cdot (\nabla U_t g_t + \nabla g_t) \\ \int_{\mathbb{R}} e^a \partial_t U_t \partial_a f_t da &= \partial_t U_t \int_{\mathbb{R}} e^a \partial_a f_t da \\ &= -\partial_t U_t \int_{\mathbb{R}} e^a f_t da = -\partial_t U_t g_t \end{aligned} \quad (41)$$

where we arrived at the second equality in the third equation by integration by parts, we deduce that

$$\partial_t g_t = \varepsilon_t \nabla \cdot (\nabla U_t g_t + \nabla g_t) - \partial_t U_t g_t, \quad g_{t=0}(x) = \rho_0(x). \quad (42)$$

The solution to this equation is not normalized for  $t \in (0, 1]$  in general. In fact

$$\partial_t \int_{\mathbb{R}^d} g_t(x) dx = - \int_{\mathbb{R}^d} \partial_t U_t(x) g_t(x) dx, \quad (43)$$

so that  $\check{\rho}_t(x) \equiv g_t(x) / \int_{\mathbb{R}^d} g_t(y) dy$  solves

$$\partial_t \check{\rho}_t = \varepsilon_t \nabla \cdot (\nabla U_t \check{\rho}_t + \nabla \check{\rho}_t) - \partial_t U_t \check{\rho}_t + \lambda_t \check{\rho}_t(x) \quad (44)$$

where we defined

$$\lambda_t = \int_{\mathbb{R}^d} \partial_t U_t(x) \check{\rho}_t(x) dx \quad (45)$$

In 44 the factor  $\lambda_t$  can be determined from the constraint that  $\int_{\mathbb{R}^d} \check{\rho}_t(x) dx = 1$ , just like  $\partial_t F_t$  in 7 can be determined from the constraint that  $\int_{\mathbb{R}^d} \rho_t(x) dx = 1$ . This means that 7 and 44 are structurally identical, and since the solutions of 7 and 44 are unique, and they are solved with the same initial condition  $\check{\rho}_0 = \rho_0$ , their solutions must coincide, i.e.  $\check{\rho}_t = \rho_t$ . In turns this means that 9 holds. Since 10 and 11 are the SDE/ODE associated with the FPE 8, 12 holds.  $\square$

**Proposition 2** (Sampling with perfect additional transport.). *Let  $b_t(x)$  be a solution to 13 and let  $X_t^b$  satisfy the SDE*

$$dX_t^b = -\varepsilon_t \nabla U(X_t^b) dt + b_t(X_t^b) dt + \sqrt{2\varepsilon_t} dW_t, \quad X_0^b \sim \rho_0, \quad (15)$$

where  $\varepsilon_t \geq 0$  is a time-dependent diffusion coefficient and  $W_t \in \mathbb{R}^d$  is the Wiener process. Then  $\rho_t(x)$  is the PDF of  $X_t^b$ , i.e. for all  $t \in [0, 1]$  and, given any test function  $h : \mathbb{R}^d \rightarrow \mathbb{R}$ , we have

$$\int_{\mathbb{R}^d} h(x) \rho_t(x) dx = \mathbb{E}[h(X_t^b)], \quad (16)$$

where the expectation on the right-hand side is taken over the law of  $(X_t^b)$ .

*Proof.* If  $b_t$  satisfies 13, then  $\rho_t$  satisfies the FPE 14. Since 15 is the SDE associated with this FPE, 16 holds.  $\square$

**Proposition 3** (Nonequilibrium Transport Sampler (NETS)). *Let  $(X_t^{\hat{b}}, A_t^{\hat{b}})$  solve the coupled system of SDE/ODE*

$$dX_t^{\hat{b}} = -\varepsilon_t \nabla U(X_t^{\hat{b}}) dt + \hat{b}_t(X_t^{\hat{b}}) dt + \sqrt{2\varepsilon_t} dW_t, \quad X_0^{\hat{b}} \sim \rho_0, \quad (19)$$

$$dA_t^{\hat{b}} = \nabla \cdot \hat{b}_t(X_t^{\hat{b}}) dt - \nabla U_t(X_t^{\hat{b}}) \cdot \hat{b}_t(X_t^{\hat{b}}) dt - \partial_t U_t(X_t^{\hat{b}}) dt, \quad A_0^{\hat{b}} = 0, \quad (20)$$

where  $\varepsilon_t \geq 0$  is a time-dependent diffusion coefficient and  $W_t \in \mathbb{R}^d$  is the Wiener process. Then for all  $t \in [0, 1]$  and any test function  $h : \mathbb{R}^d \rightarrow \mathbb{R}$ , we have

$$\int_{\mathbb{R}^d} h(x) \rho_t(x) dx = \frac{\mathbb{E}[e^{A_t^{\hat{b}}} h(X_t^{\hat{b}})]}{\mathbb{E}[e^{A_t^{\hat{b}}}]}, \quad (21)$$

where expectation at the right-hand side is taken over the law of  $(X_t^{\hat{b}}, A_t^{\hat{b}})$ .

*Proof.* We can follow the same steps as in the proof of Proposition 1 by replacing  $\varepsilon_t \nabla U_t$  by  $\varepsilon \nabla U_t - b_t$  and  $-\partial_t U_t$  by  $\nabla \cdot \hat{b}_t - \nabla U_t - \partial_t U_t$ .  $\square$

**Proposition 4** (PINN objective). *Given any  $T \in (0, 1]$  and any PDF  $\hat{\rho}_t(x) > 0$  consider the objective for  $(\hat{b}, \hat{F})$  given by:*

$$L_{PINN}^T[\hat{b}, \hat{F}] = \int_0^T \int_{\mathbb{R}^d} |\nabla \cdot \hat{b}_t(x) - \nabla U_t(x) \cdot \hat{b}_t(x) - \partial_t U_t(x) + \partial_t \hat{F}_t|^2 \hat{\rho}_t(x) dx dt. \quad (25)$$

Then  $\min_{\hat{b}, \hat{F}} L_{PINN}^T[\hat{b}, \hat{F}] = 0$ , and all minimizers are such that  $F_t$  is the free energy 3 and  $b_t(x)$  solves 23 for all  $t \in [0, T]$ .

*Proof.* Clearly the minimum value of 25 is zero and the minimizing pair  $(\hat{b}, \hat{F})$  must satisfy

$$\nabla \cdot \hat{b}_t - \nabla U_t \cdot \hat{b}_t - \partial_t U_t + \partial_t \hat{F}_t = 0 \quad (46)$$

By multiplying both sides of this equation by  $\rho_t$  it can be written as

$$\nabla \cdot (\hat{b}_t \rho_t) - \partial_t U_t \rho_t + \partial_t \hat{F}_t \rho_t = 0 \quad (47)$$

This equation requires a solvability condition obtained by integrating it over  $\mathbb{R}^d$ . This gives

$$-\int_{\mathbb{R}^d} \partial_t U_t(x) \rho_t(x) dx + \partial_t \hat{F}_t = 0, \quad (48)$$

which, by 4, implies that  $\partial_t \hat{F}_t = \partial_t F_t$ . In turn, this implies that 47 is equivalent to 13, i.e.  $\hat{b}_t$  solves 13.  $\square$

**Proposition 5** (KL control). *Let  $\hat{\rho}_t$  be the solution to the transport equation*

$$\partial_t \hat{\rho}_t = -\nabla \cdot (\hat{b}_t \rho_t), \quad \hat{\rho}_{t=0} = \rho_0 \quad (26)$$

where  $\hat{b}_t(x)$  is some predefined velocity field. Then, given any estimate  $\hat{F}_t$  of the exact free energy  $F_t$ , we have

$$D_{\text{KL}}(\hat{\rho}_{t=1} || \rho_1) \leq \sqrt{L_{\text{PINN}}^{T=1}(\hat{b}, \hat{F})}. \quad (27)$$

*Proof.* Consider

$$D_{\text{KL}}(\hat{\rho}_t || \rho_t) = \int_{\mathbb{R}^d} \log \left( \frac{\hat{\rho}_t(x)}{\rho_t(x)} \right) \hat{\rho}_t(x) dx \quad (49)$$

where  $\hat{\rho}_t$  satisfies 26. Taking the time-derivative of this expression we deduce that (using 26,  $\rho_t(x) = e^{-U_t(x)+F_t}$ , and multiple integrations by parts)

$$\begin{aligned} \frac{d}{dt} D_{\text{KL}}(\hat{\rho}_t || \rho_t) &= \int_{\mathbb{R}^d} \left[ \log \left( \frac{\hat{\rho}_t(x)}{\rho_t(x)} \right) \partial_t \hat{\rho}_t(x) - \frac{\partial_t \rho_t(x)}{\rho_t(x)} \hat{\rho}_t(x) \right] dx \\ &= \int_{\mathbb{R}^d} \left[ -\log \left( \frac{\hat{\rho}_t(x)}{\rho_t(x)} \right) \nabla \cdot (\hat{b}_t(x) \hat{\rho}_t(x)) + (\partial_t U_t(x) - \partial_t F_t) \hat{\rho}_t(x) \right] dx \\ &= \int_{\mathbb{R}^d} \left[ \hat{b}_t(x) \cdot \nabla \log \left( \frac{\hat{\rho}_t(x)}{\rho_t(x)} \right) + \partial_t U_t - \partial_t F_t \right] \hat{\rho}_t(x) dx \quad (50) \\ &= \int_{\mathbb{R}^d} \left[ \hat{b}_t(x) \cdot \nabla \hat{\rho}_t(x) + (\hat{b}_t(x) \cdot \nabla U_t(x) + \partial_t U_t - \partial_t F_t) \rho_t(x) \right] dx \\ &= \int_{\mathbb{R}^d} \left[ -\nabla \cdot \hat{b}_t(x) + \hat{b}_t(x) \cdot \nabla U_t(x) + \partial_t U_t - \partial_t F_t \right] \rho_t(x) dx \end{aligned}$$

Therefore

$$\begin{aligned} D_{\text{KL}}(\hat{\rho}_{t=1} || \rho_1) &= \int_0^1 \int_{\mathbb{R}^d} \left[ -\nabla \cdot \hat{b}_t(x) + \hat{b}_t(x) \cdot \nabla U_t(x) + \partial_t U_t - \partial_t F_t \right] \rho_t(x) dx dt \\ &\leq \left[ \int_0^1 \int_{\mathbb{R}^d} \left| -\nabla \cdot \hat{b}_t(x) + \hat{b}_t(x) \cdot \nabla U_t(x) + \partial_t U_t - \partial_t F_t \right|^2 \rho_t(x) dx dt \right]^{1/2} \quad (51) \\ &= \sqrt{L_{\text{PINN}}^{T=1}(\hat{b}, F)} \\ &\leq \sqrt{L_{\text{PINN}}^{T=1}(\hat{b}, \hat{F})} \end{aligned}$$

where the last equality holds for any  $\hat{F}$  since  $F$  is the minimizer.  $\square$

**Proposition 6** (Action Matching objective). *Given any  $T \in (0, 1]$  consider the objective for  $\hat{\phi}_t(x)$ :*

$$L_{\text{AM}}^T[\hat{\phi}] = \int_0^T \int_{\mathbb{R}^d} \left[ \frac{1}{2} |\nabla \hat{\phi}_t(x)|^2 + \partial_t \phi_t(x) \right] \rho_t(x) dx dt + \int_{\mathbb{R}^d} [\phi_0(x) \rho_0(x) - \phi_T(x) \rho_T(x)] dx. \quad (29)$$

Then the minimizer  $\phi_t(x)$  of 25 is unique (up to a constant) and  $b_t(x) = \nabla \phi_t(x)$  satisfies 13 for all  $t \in [0, T]$ .

*Proof.* By integrating by parts in time the term involving  $\partial_t \phi_t$  in the AM objective 52, we can express is as

$$L_{\text{AM}}^T[\hat{\phi}] = \int_0^T \int_{\mathbb{R}^d} \left[ \frac{1}{2} |\nabla \hat{\phi}_t(x)|^2 \rho_t(x) - \phi_t(x) \partial_t \rho_t(x) \right] dx dt. \quad (52)$$

This is a convex objective in  $\hat{\phi}$  whose minimizers satisfy

$$\nabla \cdot (\nabla \hat{\phi}_t \rho_t) = -\partial_t \rho_t. \quad (53)$$

This is 13 written in terms of  $b_t(x) = \nabla \phi_t(x)$ . The solution of this equation is unique up to a constant by the Fredholm alternative since its right hand-side satisfies the solvability condition  $\int_{\mathbb{R}^d} \partial_t \rho_t(x) dx = 0$ .  $\square$



---

**Algorithm 1** Training: Note that for both objectives the resultant set of walkers across time slices  $\{x_k^i\}$  are detached from the computational graph when taking a gradient step (*off-policy learning*).

---

- 1: **Initialize:**  $n$  walkers,  $x_0 \sim \rho_0$ ,  $A_0 = 0$ ,  $K$  time steps, model parameters for  $\{\hat{b}_t, \hat{F}_t\}$  or  $\hat{\phi}_t$  respectively, diffusion coefficient  $\varepsilon_t$ , learning rate  $\eta$
  - 2: **repeat**
  - 3:   Randomize time grid:  $t_0, t_1, \dots, t_K \sim \text{Uniform}(0, T)$ , sort such that  $t_0 < t_1 < \dots < t_K$
  - 4:   **for**  $k = 0, \dots, K$  **do**
  - 5:      $\Delta t_k = t_{k+1} - t_k$
  - 6:     **for** each walker  $i = 1, \dots, n$  **do**
  - 7:        $x_{t_{k+1}}^i = x_{t_k}^i - \varepsilon_k \nabla U_{t_k}(x_{t_k}^i) \Delta t_k + \hat{b}_{t_k}(x_{t_k}^i) \Delta t_k + \sqrt{2\varepsilon_k} \Delta W_k^i$
  - 8:        $A_{t_{k+1}}^i = A_{t_k}^i - \partial_t U_{t_k}(x_{t_k}^i) \Delta t_k - \hat{b}_{t_k}(x_{t_k}^i) \cdot \nabla U_{t_k}(x_{t_k}^i) \Delta t_k + \nabla \cdot \hat{b}_{t_k}(x_{t_k}^i) \Delta t_k$
  - 9:     **end for**
  - 10:   **end for**
  - 11:   Take gradient descent step on 33 or 34, respectively, by replacing the expectation by an empirical average over the  $n$  walkers and the time integral by an empirical average over  $t_0, \dots, t_K$ .
  - 12: **until** converged
- 

**Derivation of 30.** If  $\hat{b}_t(x) = \nabla \hat{\phi}_t(x)$ , the SDEs 19 and 20 reduce to

$$dX_t^{\hat{b}} = -\varepsilon_t \nabla U(X_t^{\hat{b}}) dt + \hat{\nabla} \phi_t(X_t^{\hat{b}}) dt + \sqrt{2\varepsilon_t} dW_t, \quad \hat{X}_0^{\hat{b}} \sim \rho_0, \quad (54)$$

$$dA_t^{\hat{b}} = \Delta \hat{\phi}_t(X_t^{\hat{b}}) dt - \nabla U_t(X_t^{\hat{b}}) \cdot \nabla \hat{\phi}_t(X_t^{\hat{b}}) dt - \partial_t U_t(X_t^{\hat{b}}) dt, \quad A_0^{\hat{b}} = 0, \quad (55)$$

Since by Itô formula we have

$$\begin{aligned} d\hat{\phi}_t(X_t^{\hat{b}}) &= \partial_t \hat{\phi}_t(X_t^{\hat{b}}) dt - \varepsilon_t \nabla \hat{\phi}_t(X_t^{\hat{b}}) \cdot \nabla U(X_t^{\hat{b}}) dt + |\nabla \hat{\phi}_t(X_t^{\hat{b}})|^2 dt \\ &\quad + \sqrt{2\varepsilon_t} \nabla \hat{\phi}_t(X_t^{\hat{b}}) \cdot dW_t + \varepsilon_t \Delta \hat{\phi}_t(X_t^{\hat{b}}) dt, \end{aligned} \quad (56)$$

we can express

$$\begin{aligned} \Delta \hat{\phi}_t(X_t^{\hat{b}}) dt &= \frac{1}{\varepsilon_t} d\hat{\phi}_t(X_t^{\hat{b}}) dt - \frac{1}{\varepsilon_t} \partial_t \hat{\phi}_t(X_t^{\hat{b}}) dt + \nabla \hat{\phi}_t(X_t^{\hat{b}}) \cdot \nabla U(X_t^{\hat{b}}) dt \\ &\quad - \frac{1}{\varepsilon_t} |\nabla \hat{\phi}_t(X_t^{\hat{b}})|^2 dt - \sqrt{\frac{2}{\varepsilon_t}} \nabla \hat{\phi}_t(X_t^{\hat{b}}) \cdot dW_t. \end{aligned} \quad (57)$$

If we insert this expression in the SDE 55, we can write it as

$$dA_t^{\hat{b}} = \frac{1}{\varepsilon_t} d\hat{\phi}_t(X_t^{\hat{b}}) dt + dB_t. \quad (58)$$

where  $dB_t$  is given by 31. Integrating 58 gives 30.

## 5.2 DETAILS ON NUMERICAL EXPERIMENTS

In the following we include details for reproducing the experiments presented in Section 4. An overview of the training procedure is given in Algorithm 1. Note that the SDE for the weights can be replaced with 30 when learning with  $\hat{\phi}_t$ , as one would do with the action matching loss 29.

### 5.3 40-MODE GMM

The 40-mode GMM is defined with the mean vectors given as:

---

$\mu_1 = (-0.2995, 21.4577),$	$\mu_2 = (-32.9218, -29.4376),$
$\mu_3 = (-15.4062, 10.7263),$	$\mu_4 = (-0.7925, 31.7156),$
$\mu_5 = (-3.5498, 10.5845),$	$\mu_6 = (-12.0885, -7.8626),$
$\mu_7 = (-38.2139, -26.4913),$	$\mu_8 = (-16.4889, 1.4817),$
$\mu_9 = (15.8134, 24.0009),$	$\mu_{10} = (-27.1176, -17.4185),$
$\mu_{11} = (14.5287, 33.2155),$	$\mu_{12} = (-8.2320, 29.9325),$
$\mu_{13} = (-6.4473, 4.2326),$	$\mu_{14} = (36.2190, -37.1068),$
$\mu_{15} = (-25.1815, -10.1266),$	$\mu_{16} = (-15.5920, 34.5600),$
$\mu_{17} = (-25.9272, -18.4133),$	$\mu_{18} = (-27.9456, -37.4624),$
$\mu_{19} = (-23.3496, 34.3839),$	$\mu_{20} = (17.8487, 19.3869),$
$\mu_{21} = (2.1037, -20.5073),$	$\mu_{22} = (6.7674, -37.3478),$
$\mu_{23} = (-28.9026, -20.6212),$	$\mu_{24} = (25.2375, 23.4529),$
$\mu_{25} = (-17.7398, -1.4433),$	$\mu_{26} = (25.5824, 39.7653),$
$\mu_{27} = (15.8753, 5.4037),$	$\mu_{28} = (26.8195, -23.5521),$
$\mu_{29} = (7.4538, -31.0122),$	$\mu_{30} = (-27.7234, -20.6633),$
$\mu_{31} = (18.0989, 16.0864),$	$\mu_{32} = (-23.6941, 12.0843),$
$\mu_{33} = (21.9589, -5.0487),$	$\mu_{34} = (1.5273, 9.2682),$
$\mu_{35} = (24.8151, 38.4078),$	$\mu_{36} = (-30.8249, -14.6588),$
$\mu_{37} = (15.7204, 33.1420),$	$\mu_{38} = (34.8083, 35.2943),$
$\mu_{39} = (7.9606, -34.7833),$	$\mu_{40} = (3.6797, -25.0242)$

These means follow the definition given in the FAB (Midgley et al., 2023) code base that has been subsequently used in recent papers.

#### 5.4 NEAL'S 10- $d$ FUNNEL

The Neal's Funnel distribution is a 10- $d$  probability distribution defined as

$$x_0 \sim \mathcal{N}(0, \sigma^2), \quad x_{1:9} \sim \mathcal{N}(0, e^{x_0}) \quad (59)$$

where  $\sigma = 3$  and we use subscripts here as a dimensional index and not as a time index like in the rest of the paper. Following this, we use as a definition of the interpolating potential:

$$U_t(x) = \frac{1}{2}x_0^2(1-t + \frac{t}{\sigma^2}) + \frac{1}{2} \sum_{i=1}^{d-1} e^{-tx_0} x_i^2 + (d-1)tx_0 \quad (60)$$

so that at  $t = 0$ , we have  $U_0(x) = \frac{1}{2}x_0^2 + \frac{1}{2} \sum_{i=1}^{d-1} x_i^2$  and at time  $t = 1$  we have the funnel potential given as  $U_1(x) = \frac{1}{2\sigma^2}x_0 + \frac{1}{2} \sum_{i=1}^{d-1} e^{-x_0} x_i^2 + (d-1)x_0$ .

#### 5.5 PERFORMANCE METRICS

**Effective sample size.** We can compute the self-normalized ESS as

$$\text{ESS}_t = \frac{\left( N^{-1} \sum_{i=1}^N \exp(A_t^i) \right)^2}{N^{-1} \sum_{i=1}^N \exp(2A_t^i)} \quad (61)$$

at time  $t$  along the SDE trajectory. We can use the ESS both as a quality metric and as a trigger for when to perform resampling of the walkers based on the weights, using, e.g. systematic resampling (Doucet et al., 2001; Bolić et al., 2004). Systematic resampling is one of many resampling techniques from particle filtering wherein some walkers are killed and some are duplicated based on their importance weights. These

**2-Wasserstein distance** . The 2-Wasserstein distance reported in Table 1 were computed with 2000 samples from the model and the target density using the Python Optimal Transport library.

**Maximum Mean Discrepancy (MMD)** . We use the MMD following Blessing et al. (2024) to benchmark the performance of NETS on Neal’s funnel. We use the definition of the MMD as

$$\text{MMD}^2(\hat{\rho}, \rho) \approx \frac{1}{n(n-1)} \sum_{i,j} k(\hat{x}_i, \hat{x}_j) + \frac{1}{m(m-1)} \sum_{i,j} k(x_i, x_j) - \frac{2}{nm} \sum_i \sum_j k(\hat{x}_i, x_j) \quad (62)$$

where  $\hat{x} \sim \hat{\rho}$  is from the model distribution and  $x \sim \rho$  is from the target and  $k : \mathbb{R}^d \times \mathbb{R}^d \rightarrow R$  is chosen to be the radial basis kernel with unit bandwidth.

### 5.5.1 DETAILS ON $\phi^4$ THEORY

We consider the Euclidean scalar  $\phi^4$  theory given by the action

$$S_{\text{Euc}}[\varphi] = \int [\partial_\mu \varphi(x) \partial^\mu \varphi(x) + m^2 \varphi^2(x) + \lambda \varphi^4(x)] d^D x \quad (63)$$

where we use Einstein summation to denote the dot product with respect to the Euclidean metric and  $D$  is the spacetime dimension. We are interested in acquiring a variant of this expression that provides a fast computational realization when put onto the lattice. Using Green’s identity (integrating by parts) we note that

$$\int (\partial_\mu \varphi(x) \partial^\mu \varphi(x)) d^d x = \int \partial_\mu \varphi \cdot \partial_\mu \varphi d^d x = - \int \varphi(x) \partial_\mu \partial^\mu \varphi(x) d^d x + \text{vanishing surface term} \quad (64)$$

so that

$$S_{\text{Euc}}[\varphi] = \int -\varphi(x) \partial_\mu \partial^\mu \varphi(x) + m^2 \varphi^2(x) + \lambda \varphi^4(x) d^d x. \quad (65)$$

Discretizing  $S_{\text{Euc}}$  onto the lattice

$$\Lambda = \{a(n_0, \dots, n_{d-1}) \mid n_i \in \{0, 1, 2, \dots, L\}, i = 0, 1, \dots, d, a \in \mathbb{R}_+\},$$

where  $a$  is the lattice spacing used to define the physical point  $x = an$ , we use the forward difference operator to define

$$\partial_\mu \varphi(x) \rightarrow \frac{1}{a} [\varphi(x + \mu) - \varphi(x)] \quad \partial_\mu \partial^\mu \varphi(x) \rightarrow \frac{1}{a^2} [\varphi(x + \mu) - 2\varphi(x) + \varphi(x - \mu)]. \quad (66)$$

Using these expressions, we write the discretized lattice action as

$$S_{\text{Lat}} = \sum_{x \in \Lambda} a^D \left[ \sum_{\mu=1}^D -\frac{1}{a^2} [\varphi_{x+\mu} \varphi_x - 2\varphi_x^2 + \varphi_{x-\mu} \varphi_x] + m^2 \varphi_x^2 + \lambda \varphi_x^4 \right] \quad (67)$$

$$= \sum_x a^D \left[ 2Da^{-2} \varphi_x^2 - a^{-2} \sum_\mu [\varphi_{x+\mu} \varphi_x + \varphi_{x-\mu} \varphi_x] + m^2 \varphi_x^2 + \lambda \varphi_x^4 \right] \quad (68)$$

$$= \sum_x a^d \left[ 2Da^{-2} \varphi_x^2 - 2a^{-2} \sum_\mu [\varphi_x \varphi_{x+\mu}] + m^2 \varphi_x^2 + \lambda \varphi_x^4 \right] \quad (69)$$

$$= \sum_x a^D \left[ -2a^{-2} \sum_\mu \varphi_x \varphi_{x+\mu} + (2a^{-2}D + m^2) \varphi_x^2 + \lambda \varphi_x^4 \right] \quad (70)$$

where we have used the fact that on the lattice  $\sum_x \varphi_x \varphi_{x+\hat{\mu}} = \sum_x \varphi_{x-\hat{\mu}} \varphi_x$  to get the third equality. It is useful to put the action in a form that is independent of the lattice spacing  $a$ . To do so, we introduce the re-scaled lattice field as

$$\varphi_x \rightarrow a^{D/2-1} \varphi_x, \quad m^2 \rightarrow a^2 m^2, \quad \text{and} \quad \lambda \rightarrow a^{4-D} \lambda. \quad (71)$$

Plugging these rescalings into 70 gives us the final expression

$$S_{\text{Lat}} = \sum_x \left[ -2 \sum_\mu \varphi_x \varphi_{x+\mu} \right] + (2D + m^2) \varphi_x^2 + \lambda \varphi_x^4, \quad (72)$$

which we are to use in simulation.

### 5.5.2 FREE THEORY $\lambda = 0$

Turning off the interaction makes it possible to analytically solve the theory. To do this, introduce the discrete Fourier transform relations

$$\varphi_k = \frac{1}{\sqrt{L^D}} \sum_x \varphi_x e^{-ik \cdot x} \quad (73)$$

$$\varphi_x = \frac{1}{\sqrt{L^D}} \sum_k \varphi_k e^{ik \cdot x} \quad (74)$$

for discrete wavenumbers  $k = \frac{2l\pi}{L}$  with  $l = 0, \dots, L-1$ . Plugging in 74 into the first part of 70, we get the expanded sum

$$\sum_x \left[ -2 \sum_\mu \hat{\varphi}_x \hat{\varphi}_{x+\mu} \right] \rightarrow -\frac{2}{L^d} \sum_x \sum_\mu \sum_k \sum_{k'} \varphi_k \varphi_{k'} e^{i(k+k') \cdot x} e^{ik' \cdot \mu} \quad (75)$$

$$= -2 \sum_\mu \sum_k \sum_{k'} \delta_{k, -k'} \varphi_k \varphi_{k'} e^{ik' \cdot \mu} \quad (76)$$

$$= -2 \sum_\mu \sum_k \varphi_k \varphi_{-k} e^{-ik \cdot \mu} \quad (77)$$

$$= -2 \sum_\mu \sum_k \varphi_k \varphi_{k^*} e^{-ik \cdot \mu} \quad (78)$$

$$= -2 \sum_\mu \sum_k |\varphi_k|^2 [\cos k_\mu + i \sin k_\mu] = - \sum_\mu \sum_k |\varphi_k|^2 \cos k_\mu \quad (79)$$

where  $\phi^*$  indicates conjugation, and we got the first equality by the orthogonality of the Fourier modes, the second by the Kronecker delta, and the third by the reality of the scalar field. Proceeding similarly for the terms proportional to  $\varphi^2$  gives us the expression

$$S_k = \sum_k \left[ m^2 + 2D - 2 \sum_\mu \cos k_\mu \right] |\varphi|^2 \quad (80)$$

The above equation can be written in quadratic form to highlight that the field may be sampled analytically

$$S_k = \frac{1}{L^d} \sum_k \varphi_k M_{k, -k} \varphi_{-k} \quad (81)$$

$$\text{where } M_{k, -k} = \left[ m^2 + 2D - 2 \sum_\mu \cos k_\mu \right] \delta_{k, -k} \quad (82)$$

Note that this free theory can be sampled for any  $m^2 > 0$ .

### 5.5.3 $\varphi^4$ NUMERICAL DETAILS

We numerically realize the above lattice theory in D=2 spacetime dimensions. We use an interpolating potential with time dependent  $m_t^2 = (1-t)m_0^2 + tm_1^2$ ,  $\lambda_t = (1-t)\lambda_0 + t\lambda_1$  where  $\lambda_0$  is always chosen to be 0 (though we note that you could run this sampler for any  $U_0$  that you could sample from easily, not just analytically but also with existing MCMC methods). For the  $L = 20$  ( $d = L \times L = 400$  dimensional) experiments, we identify the critical point of the theory (where the lattices go from ordered to disordered) using HMC by studying the distribution of the magnetization of the field configurations as  $M[\varphi^i(x)] = \sum_x \varphi^i(x)$ , where summation is taken over all lattice sites on the  $i^{\text{th}}$  lattice configuration. We identify this at  $m_1^2 = -1.0$ ,  $\lambda_1 = 0.9$  and use these as the target theory parameters on which to perform the sampling. For the  $L = 16$  test ( $d = 256$ ), we go past this phase transition into the ordered phase of the theory, which we identify via HMC simulations at  $m_1^2 = -1.0$ ,  $\lambda_1 = 0.8$ .